

Cite this: *Soft Matter*, 2012, **8**, 2915

www.rsc.org/softmatter

PAPER

Multidrug resistance protein P-glycoprotein does not recognize nanoparticle C₆₀: experiment and modeling†

Xue Xu,^{‡a} Ruibin Li,^{‡b} Ming Ma,^a Xia Wang,^a Yonghua Wang^{*a} and Hanfa Zou^{*b}

Received 22nd September 2011, Accepted 9th December 2011

DOI: 10.1039/c2sm06811g

Organisms have evolved stress-inducible defense responses such as the P-glycoprotein (P-gp)-mediated efflux system to maintain chemical homeostasis in cells for both endogenous and xenobiotic compounds. However, despite the extensive focus on the potential interactions of P-gp with small molecules, the effect of nanoparticles on this transporter is scarcely reported. Thus in this work, *in vitro* experiments combined with molecular dynamics (MD) simulations were carried out to investigate the interactions of the multidrug resistance (MDR) protein P-gp with fullerene (C₆₀), one of the most important nano-drug carriers. Upon exposure to fluorescence-labeled C₆₀ (0–70 μg mL⁻¹) for 2 h, significant accumulation of C₆₀ is found in both the K562S and K562R cells, suggesting the incapability of P-gp to induce the efflux of this nanoparticle. In addition, *in vitro* inhibition assays also reveal that C₆₀ does not obviously hinder P-gp-mediated rhodamine-123 transport in both K562S and K562R cells. The theoretical simulations further reveal the mechanism involved in C₆₀-P-gp interactions, *i.e.*, the binding of C₆₀ barely induces the conformational changes of P-gp with RMSD of ~4.8 Å and radius of gyration of ~41.5 Å, and also no theoretical evidence shows that the C₆₀ acts as a substrate or inhibitor of P-glycoprotein. These results demonstrate the potential of C₆₀ as a good carrier candidate for MDR-targeted drug delivery, since organisms probably have not evolved to recognize this nanoparticle.

1. Introduction

Living organisms have been coping with xenobiotics since life began and, as life has evolved, changes have been made by cells in response to adverse environmental changes. For example, organisms develop defense systems allowing them to survive during evolution.¹ This is a (near) ubiquitous rule of organisms to adapt to environmental stress. Unfortunately, this apparently ideal system delivers a death blow to current chemotherapy for tumors, since some tumors are inherently resistant to the majority of chemotherapeutic drugs (*i.e.* intrinsic resistance), whereas many others present broad-spectrum, or multidrug resistance (MDR) after several rounds of chemotherapy (*i.e.* acquired resistance).² Such a depressing fact of tumor cells insensitive to structurally diverse drugs with disparate intracellular targets was subsequently discovered to be related with the overexpression of a large (170 kD) cell-surface molecule, P-

glycoprotein (P-gp), encoded by the human MDR1 gene is the major cause of intrinsic or acquired MDR.

As a typical member of the ABC (ATP-binding cassette) superfamily of active transporters, P-gp is highly localized in the kidneys, adrenal gland, liver, colon and lung, and also at basal level in the prostate, skin, spleen, heart, skeletal muscle, stomach and ovary³ where the normal function involves the excretion of drugs and their metabolites. CDNA sequence analysis has further confirmed a remarkable degree of homology between different P-gp gene family members within a species and across species. The vertebrate human being, mouse and hamster P-gps^{4–6} have approximately 50% to 65% homology with P-gp from other species, such as the invertebrate sea urchin P-gp,⁷ and even the plant *Arabidopsis thaliana* P-gp,⁸ suggesting that these P-gp genes are undergoing concerted evolution. As one important contributor to MDR, the expression of functional P-gp enable a reduction in drug accumulation and increased drug resistance, and thus, the development of P-gp inhibitors, or drugs that could circumvent efflux by P-gp, would be critical for the successful treatment of MDR tumors. However, although previous trials were performed to develop a variety of functionalized small molecules,^{9–11} the effect of nanoparticles, the potentially most important players in drug delivery systems, on this transporter is scarcely reported.

Nanoparticles, characterized by a nanometre-size scale, have a very high surface area and high percentages of component atoms on the surface, and are expected to impact almost every

^aCollege of Life Sciences, Northwest A&F University, Yangling, 712100, Shaanxi, China. E-mail: yh_wang@nwsuaf.edu.cn; Tel: +86 029 87092262

^bNational Chromatographic R&A Center, CAS Key Laboratory of Separation Sciences for Analytical Chemistry, Dalian Institute of Chemical Physics, Chinese Academy of Sciences (CAS), 116023 Dalian, China. E-mail: hanfazou@dicp.ac.cn

† Electronic supplementary information (ESI) available. See DOI: 10.1039/c2sm06811g

‡ contributed equally

industrial and manufacturing sector in the 21st century, including medicine for the purpose of diagnosis, imaging, and drug delivery.^{12,13} As an important area of research in modern material nanoscience, carbon-based materials and their relationship with the biological systems have received great attention of scientists, physicians, industrialists across the world, among which fullerenes take one of the first places.¹⁴ The fullerene family, especially C₆₀, has many potential applications based on their unique free radical chemistry and antioxidant properties, including inhibiting HIV-1 protease, scavenging free radicals, producing singlet oxygen by energy transfer with high quantum yield to cleave DNA, identifying protein signatures for pathologies and biomarker discovery, as well as bringing forth new drug delivery systems for diagnosis and therapy.¹⁴ Although C₆₀ has existed on earth for more than 1,000 years, it only occurs in the environment from natural and anthropogenic sources such as forest fires, volcanic eruptions and the combustion of carbon-based materials.¹⁵ Due to the scarce resources of C₆₀, this nanoparticle seems to be incapable of acting as “a privileged structure” selected by evolutionary pressure to interact with a wide array of biological targets as other natural products,¹⁶ but probably represents an evolutionary obstacle for its hosts. If our speculation succeeds, the living organisms under external stress (C₆₀ exposure) will not have the relevant measures to cope with both the current and potential environmental demands; much less trigger the activation of cellular defense systems against this nanoparticle. To validate this viewpoint, we thus employed a combined experimental and theoretical approach in this work to assess the interaction of C₆₀ with P-gp, the most prevalent factor for systemic clearance and limiting the xenobiotics penetration. This helps to address the questions (1) whether P-gp functions as a defense system against C₆₀ stress; and (2) whether C₆₀ molecules can avoid recognition by the P-gp efflux pump to overcome P-gp-mediated MDR.

2. Materials and methods

Chemicals

1-(3-dimethylaminopropyl)-3-ethylcarbodiimide hydrochloride (EDC) (99.9%) and N-hydroxysuccinimide (NHS) (99.9%) were purchased from Pierce (Pierce, IL); (1,2-methanofullerene C₆₀)-61-carboxylic acid (C₆₀-C-COOH), Fluoresceinamine, isomer 1 (5-Aminofluorescein, 5-AMF), and Rhodamine 123 (Rho123) were purchased from Sigma-Aldrich; Buckminsterfullerene (C₆₀) (99.9%) was purchased from Aladdin Company (Shanghai, China).

Cell culture

Multidrug resistance (K562R) and drug-sensitive (K562S) human leukemia cells¹⁷ obtained from the Institute of Blood, Chinese Academy of Medical Sciences (Tianjin China), were seeded initially at a density of 1.0×10^4 cells mL⁻¹. All cell cultures were maintained in 75-cm² vented culture flasks at 37 °C with RPMI-1640 medium containing 10% calf serum in 5% carbon dioxide atmosphere, in which the cells were passaged at 70–80% confluency every 2–3 days.

Preparation of the 5-aminofluorescein-labeled C₆₀ (AMF-C₆₀)

AMF-C₆₀ was prepared according to our previously reported method.¹⁷ In brief, 6 mg of C₆₀-C-COOH was dissolved in 15 mL of dimethyl sulfoxide (DMSO), followed by the addition of 13 mg of NHS and 8 mg of EDC, and the mixture was shaken in a reciprocating shaker for 20 min. After that, 7 mg 5-AMF in 4 mL DMSO was added dropwise to the mixture solution under vigorous stirring. The reaction mixture at pH 9.0 was stirred at 20 °C for 24 h, and the obtained yellow–green solution was lyophilized to dryness. Subsequently, the resultant mixture was redissolved in Milli-Q water to remove the unlabeled 5-AMF by a Sephadex LH-20 gel permeation column (Solarbio Bioscience & Technology Company, Shanghai, China) with estimated sizes of 0.1 and 4 kilo-daltons. Finally, the resulting compound was collected, lyophilized to dryness, and stored at 4 °C before use. The structure of AMF-C₆₀ was identified by nanoACQUITY ultra performance liquid chromatography–quadrupole time-of-flight mass spectrometry (UPLC-Q-TOF MS, Waters Corp, Milford, America) with a peak at $m/z = 1107$.

Flow cytometry (FCM) and confocal fluorescence microscopy (CLSM)

C₆₀ recognition by P-gp was determined by FCM using the fluorescent compounds 5-AMF and Rho-123, respectively. To evaluate whether C₆₀ was a potential P-gp substrate, cells were first isolated by centrifugation and purified by three successive washes with sterile isotonic PBS, then incubated with AMF-C₆₀ in the K562R and K562S cells, respectively. Controls were prepared in the same manner as the above cellular samples except adding Milli-Q water (positive control) and 5-AMF (negative control), respectively. Similarly, cells stained with Rho-123 were mixed with C₆₀ to identify whether C₆₀ had potential to be a P-gp inhibitor. After a 2h incubation and washing, the stained samples ($ca. 1 \times 10^7$) were analyzed on a FACS Vantage SE flow cytometer from BD (Franklin Lakes, NJ) with Ar-ion ($\lambda = 488$ nm) excitation. The data was analyzed using WinMDI 2.9 Software (TSRI, La Jolla, CA). The CLSM analysis was performed by a TCS-SP2 confocal laser scanning microscope (Leica, Wetzlar, Germany) with a 40× objective.

Simulation methodology

Structural modeling of human P-gp. Homology modeling was performed to build the 3D model of human P-gp with mouse P-gp (PDB code 3G5U, chain A, resolution 3.8 Å) as a template. The sequence alignment of the target and template sequences was carried out using the ClustalW program,¹⁸ and then, the sequence was submitted to the Swiss-Model server (www.expasy.ch/swissmod) to predict the 3D model of human P-gp.¹⁹ After that, we assessed the quality of the resulting homology structure using the protein structure verification WHAT-CHECK²⁰ module of the WHATIF on-line server (<http://swift.cmbi.kun.nl/WIWWWI/modcheck.html>) to identify problematic residues, and check the Ψ and Φ bond angles in a Ramachandran plot.

System assembly. The membrane used to provide the lipid environment for the protein was constructed from a palmitoyl-oleoyl-phosphatidylcholine (POPC) membrane that consisted

of an equilibrated rectangular bilayer with 100 POPC lipids in each leaflet.²¹ Starting coordinates were obtained by expanding a previously equilibrated POPC bilayer to 274 lipids. Starting from the pure POPC bilayer, the human P-gp structure was inserted by using the VMD *Membrane* plug-in,²² with the initial membrane position along the z axis determined by matching positions of headgroups with the Leu36, Thr37, Trp694, Arg695, Ile696, Leu697, Lys698, Leu699, Asn700, Ser701, Thr702 side chains of the P-gp transmembrane domain.²³ Lipids within 0.6 Å of the protein and those located in the pore were removed. A pre-equilibrated water box was then overlaid on the protein-lipid system in order to completely hydrate the aqueous part of the protein structure. Ten chloride ions displaced ten water molecules to bring the entire system to charge neutrality. After that, the bilayer was melted with MD at 310 K, and the protein was kept frozen to keep the membrane intact. The final assembly reached 14 0000–15 0000 atoms, and an approximate system size of $90 \times 90 \times 142 \text{ \AA}^3$. The neat C_{60} carbon fullerene molecules were successively modeled. The CHARMM22 force-field parameters²⁴ were utilized to describe this nanoparticle with all carbon atoms taken to be neutral. The C–C interaction in C_{60} was described by a Lennard–Jones potential with a van der Waals diameter $\sigma_{CC} = 3.47 \text{ \AA}$ and interaction strength $\epsilon_{CC} = 0.275 \text{ kJ mol}^{-1}$.²⁵ For the active efflux of the P-gp substrate, it has been postulated that when drug substrates are added, they diffuse from the extracellular medium into the lipid bilayer and enter the solvent-filled common drug-binding pocket through portals formed by transmembrane segments (TMs) 2 and 11 and TMs 5 and 8.²³ Thus, we investigated the binding of C_{60} to P-gp through three sceneries: (a) four C_{60} molecules positioned in the extracellular regions of P-gp; (b) four C_{60} molecules placed in the intracellular regions of P-gp; and (c) four C_{60} molecules positioned in the interior region of lipid bilayers.²³ In addition, two mutant systems based on the (c) scenario were performed to further probe the interaction mode of C_{60} and P-gp, *i.e.*, (d) the system with Val165-Ala, Pro402-Ala and Arg680-Ala mutants; and (e) the system with Asp167-Ala, Val168-Ala, Gly169-Ala, Arg680-Ala, Lys681-Ala, Leu682-Ala and Ser683-Ala mutants.

Molecular simulations. MD simulations of wild-type and mutant P-gp presented in this work were carried out with the NAMD package version 2.7²⁶ for 50 and 20 ns respectively, using the CHARMM27 force field²⁷ with CMAP corrections²⁸ for the protein and the POPC membrane. The pressure was controlled at 1 atm by the Nosé–Hoover Langevin piston method, and the temperature was kept at 310 K using the Langevin friction force scheme with the damping coefficient at 5 ps^{-1} . Three-dimensional periodic boundary conditions were applied, and the long-range electrostatic interactions were assessed using the particle mesh Ewald method (PME)²⁹ with a 10 \AA cutoff for the real space calculation. Water molecules were represented as the TIP3P model. Bonds between hydrogen atoms and heavy atoms were constrained at their equilibrium lengths using the SHAKE and RATTLE algorithms.^{30,31} A time step of 2 fs was used to integrate the equations of motions. System coordinates were saved every 10 ps for data analysis. A representative snapshot of P-gp embedded in a hydrated POPC lipid bilayer is shown in Fig. S1. ESI.†

3. Results

C_{60} transport by P-gp

For evaluating whether C_{60} was a potential P-gp substrate, K562S and K562R human leukemia cells ($ca. 1 \times 10^7$) were incubated in 6-well plates containing 0, 40, 50, 60, and $70 \mu\text{g mL}^{-1}$ of AMF- C_{60} for 2 h.³² Before the assay performed, we first carried out a control experiment with 5-AMF-labeled C_{60} replaced with 5-AMF in concentrations of 1, 5, 10, $15 \mu\text{g mL}^{-1}$,³³ in order to determine whether this fluorescein is susceptible to P-gp mediated efflux transport. The fluorescence overlay histogram plots in Fig. 1A and B show the accumulation of 5-AMF in the K562R cells is comparable to that of the K562S cells, indicating that the dye transport is not affected by the expression level of P-gp. This implies that 5-AMF is not recognized and exported by the P-gp, and thereby, confirms that the data of P-gp substrate assay in this section is meaningful and reliable.

Further comparison between the geometric mean fluorescence intensity (G_{mean}) values of AMF- C_{60} in the two types of cells (Fig. 2A) reveals no significant difference except at a concentration of $0 \mu\text{g mL}^{-1}$. This result indicates that despite the notably higher P-gp expression (nearly 458 times) in the K562R cells compared to the K562S cells,¹⁷ this factor does not seem to affect the nanoparticle interaction with cells in circulation. To study the efficacy of AMF-labeled C_{60} in the drug-sensitive and -resistant cells, we studied the dose–response relationship in

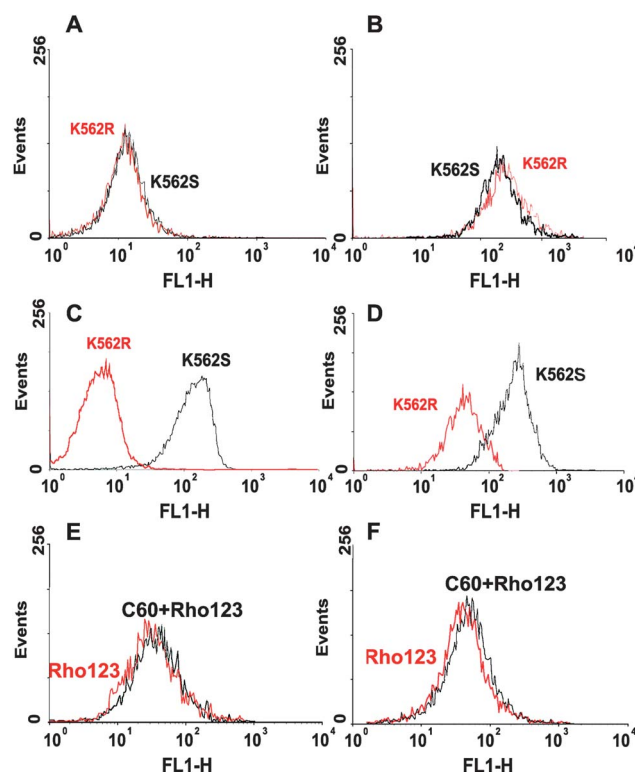


Fig. 1 The histogram of K562S and K562R cells incubated with A) $1 \mu\text{g mL}^{-1}$ of 5-AMF, B) $15 \mu\text{g mL}^{-1}$ of 5-AMF, C) $0.5 \mu\text{g mL}^{-1}$ of Rho123, D) $1.5 \mu\text{g mL}^{-1}$ of Rho-123. And the histogram of K562R incubated with $10 \mu\text{g mL}^{-1}$ of C_{60} and $1.5 \mu\text{g mL}^{-1}$ of Rho123 (E), and $40 \mu\text{g mL}^{-1}$ of C_{60} and $1.5 \mu\text{g mL}^{-1}$ of Rho123 (F).

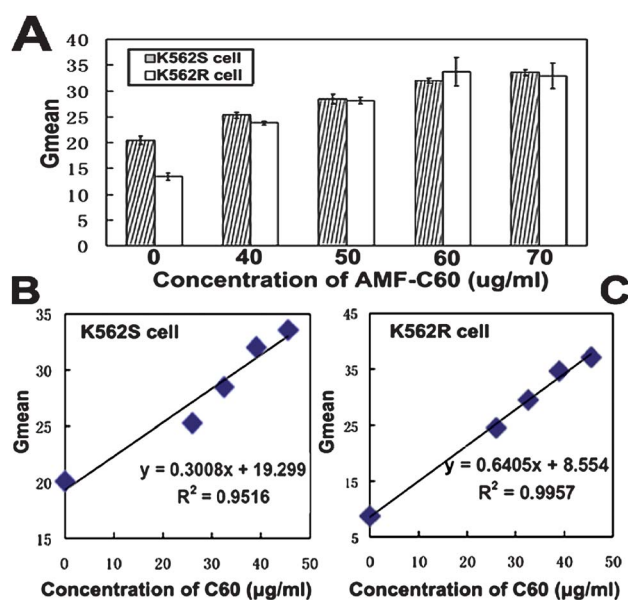


Fig. 2 (A) The fluorescence intensity (G_{mean}) values of AMF- C_{60} in K562S and K562R cells by flow cytometry analysis. The plots at the bottom show the relationship between the G_{mean} values of AMF- C_{60} and the concentration of C_{60} for K562S (B) and K562R (C), respectively.

AMF- C_{60} -induced fluorescence intensity. Fig. 2B and C show the enhancement of concentration of C_{60} corresponding to the fluorescence intensity of AMF- C_{60} in an almost linear manner (linearly dependent coefficient: $R^2 = 0.9516$ for K562S cells and $R^2 = 0.9957$ for K562R cells).

During examination of the fluorescence intensity of AMF- C_{60} under CLSM, both the drug-sensitive and multidrug resistant

K562 cells ($ca. 1 \times 10^7$) were incubated with AMF-labeled C_{60} at 0, 40, 50, 60, and 70 $\mu\text{g mL}^{-1}$ for 2 h, respectively. Fig. 3 panels A1, A2, B1 and B2 illustrate the obtained fluorescent images of K562R and K562S cells, showing that the fluorescent signals in dye-treated cells were distinctively bright compared with the black reference image, and both K562R and K562S cells display similar levels of green fluorescence. This indicates that AMF- C_{60} is definitely not susceptible to the P-gp-mediated efflux.

C_{60} inhibition on P-gp

First, we performed an accumulation assay with Rho123 to assess the effects of this fluorescent dye on P-gp efflux. Rho123, as a widely used cationic fluorescent dye, is a well established model substrate for testing the functional transport of P-gp.^{34–36} Diluted suspensions of the K562S and K562R cells ($ca. 1 \times 10^7$) were mixed with the fluorescent solution to reach a final concentration of 0.5, 1.5, 2, 5 $\mu\text{g mL}^{-1}$ of Rho123³⁷ and incubated at 37 °C for 2 h, respectively. The results of the FCM analysis in Fig. 1C and D show significant difference in cellular fluorescence ($\sim 85\%$), indicating that the low level of expression of P-gp in the K562S cells blocks the fluorescent efflux. Moreover, Fig. 3C1 and C2 shows a significant portion of Rho123 clearly localized in the cytoplasm of K562S cells. However, there was almost no Rho123 observed in the cytoplasm for K562R cells but on cell membrane. The above results thus suggest the high sensitivity and great efflux efficiency of Rho123 in the K562 cell model.

Subsequently, for assessing whether C_{60} possesses P-gp inhibition potential, we measured the accumulation of Rho123 in the presence of C_{60} in the K562 cell models. The K562R cells ($ca. 1 \times 10^7$) were incubated with C_{60} (0, 10, 20, 30, 40 $\mu\text{g mL}^{-1}$) in media containing 1.5 $\mu\text{g mL}^{-1}$ of Rho123 for 2 h with gentle shaking,

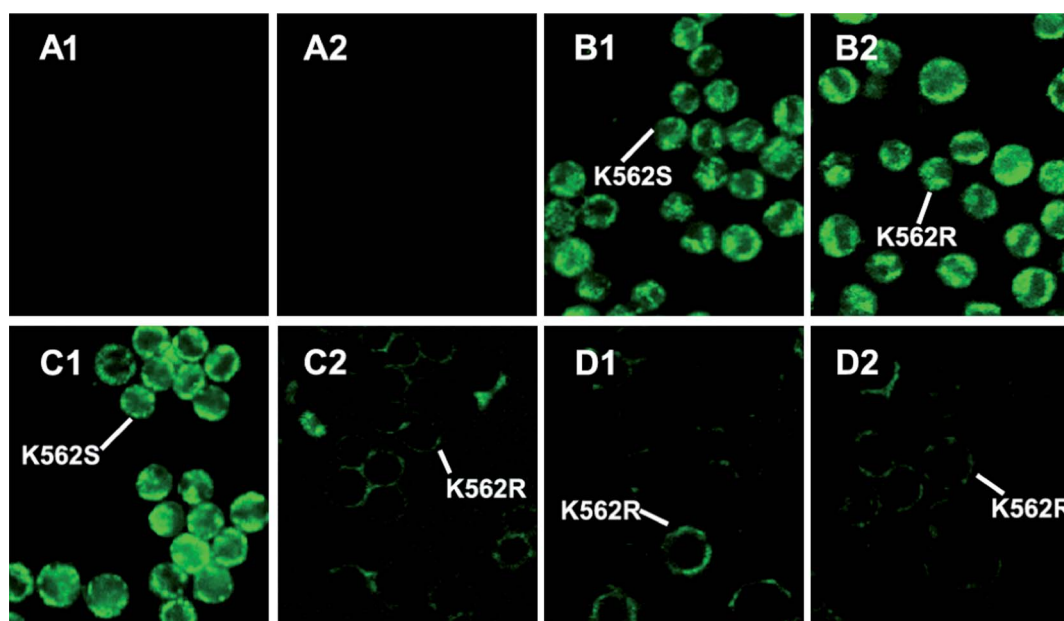


Fig. 3 Confocal microscopy images of (A1) Blank control of K562S cells; (A2) Blank control of K562R cells; (B1) K562S cells treated by 50 $\mu\text{g mL}^{-1}$ of AMF- C_{60} ; (B2) K562R cells treated by 50 $\mu\text{g mL}^{-1}$ of AMF- C_{60} ; (C1) K562S cells treated by 1.5 $\mu\text{g mL}^{-1}$ of Rho-123; (C2) K562R cells treated by 1.5 $\mu\text{g mL}^{-1}$ of Rho-123; (D1) K562R cells treated by 10 $\mu\text{g mL}^{-1}$ of C_{60} and 1.5 $\mu\text{g mL}^{-1}$ of Rho-123; (D2) K562R cells treated by 40 $\mu\text{g mL}^{-1}$ of C_{60} and 1.5 $\mu\text{g mL}^{-1}$ of Rho-123.

followed by washing 5 times with PBS to remove the unbound C_{60} . The histogram overlays depicting fluorescence intensity for the combined treatment with Rho123 and C_{60} in the K562R cells show that C_{60} lacks the ability to efflux the P-gp substrate Rho123 since the fluorescence intensity does not improve in the presence of C_{60} compared with the result from the single treatment with Rho123, and remains low ($G_{\text{mean}} = 20 \pm 5.8$) at different concentrations of C_{60} (Fig. 1E and F). This result is supported by the confocal microscopy images in Fig. 3D1 and D2, showing low retention of Rho123 (very low brightness) in the K562R cells in the presence of C_{60} .

Molecular dynamics analysis

Due to the unavailability of the X-ray structure of human P-gp, the homology modeling for the protein structure from its primary sequence was performed. The sequence and structural comparison with the template 3G5U are shown in Fig. S2, ESI†. The human and mouse P-gp proteins show a high amount of conservation, with 87% sequence identity. The backbone of the human P-gp model was superimposed with the mouse P-gp crystal structure to evaluate the reliability of our homology-modeled protein. Out of 1284 residues crystallized in the mouse P-gp structure, 1242 pairs of α -carbons were used to compute the root-mean-squared distance (RMSD) between the human model and the crystal structure. This comparison yielded an overall RMSD value less than 1.1 Å and the RMSD of secondary structure elements (SSE-RMSD) was lower than the starting value by 0.5–0.8 Å, verifying that a reliable homology model was generated. Moreover, almost all key amino acids (such as Ser222, Ile306, Leu339, Ile868, Gly872, Thr945 and Val982²³) interacting with the substrates in the binding domain are well overlaid in 3D space in the two structures. The combined results clearly suggest that the homology-modeled P-gp structure is reliable, which can be used for further molecular dynamics analysis.

After the protein-membrane system assembly, we calculated the $C\alpha$ coordinate root mean square displacement (RMSD) of the transmembrane protein P-gp relative to the original structure to monitor the quality of the MD simulations. Fig. 4 shows that in all simulations, the RMSD rapidly increases during the initial 6 ns of free equilibration, and continues to grow to ~ 4.8 Å, where it is stable for the remainder of the simulations. This result indicates that the P-gp's conformation does not seem to change appreciably in the presence of lipids, and the P-gp's

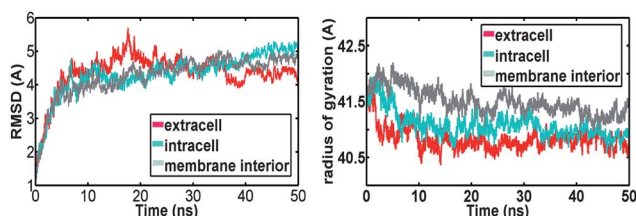


Fig. 4 (A) Time evolutions of RMSD of backbone atoms of the whole P-gp protein from the starting structure during the three 50 ns MD simulations. The red, blue, and silver curves represent the RMSD in P-gp with C_{60} placed in the extracellular region, intracellular region and in the membrane interior, respectively. (B) Time evolutions of the radius of gyration of the P-gp for the three simulated trajectories.

structural drift is approximately the same regardless of the binding of the nanoparticles located at different sites in the membrane bilayer. When the radius of gyration was estimated, a similar phenomenon was observed again: after an initial period (10 ns), the average value reaches 41.5 Å, and once more, no significant difference among the three systems is observed (Fig. 4B).

Once the stability of our systems has been demonstrated, we proceeded to analyze the propensity of C_{60} molecules to partition into the P-gp internal cavity. For the extracellular system, C_{60} molecules were initially distributed at the four diagonal sites of the bilayers, near the extracellular mouth of the P-gp (Fig. 5A and B). During the first 4 ns, the nanoparticles moved in a curved motion. Taking C_{60}^a as an example, we drew solid lines to represent the trajectory of this molecule (Fig. 5B and Fig S3, ESI†). Within the initial 2 ns, the C_{60} migrates towards the pore entrance of P-gp with a distance of ~ 9 Å every 0.3 ns, and does not appear to shuttle back and forth to a large extent ($<20\%$). Once the distance between the C_{60}^a and the protein reduces to 8 Å, the molecule seems to stumble at every step, and moves by a roundabout route with a large degree ($>80\%$). Subsequently, the small molecules passively partitioned into the bilayer (~ 5 Å) on the basis of their affinity for the hydrophobic lipids of the membrane while flanking aromatic backbones were positioned near. In the following 45 ns, the C_{60} s seemed to be glued and fixed in the hydrophobic core regions of membrane, and thus, were not able to enter the internal drug-binding pocket through the two open portals. For example, the hydrophobic residues Leu214, Val217, Tyr316 and Leu320 located at the top of TM4 and the bottom of TM5 twist outside ($\sim 20^\circ$) after the entry of C_{60}^b into the membrane (Fig. 6A). The four residues act as fingers to capture the small molecule, and thus prevent its translation into the portal formed by TMs 4 and 6 that allow access for permeation of drug molecules directly from the bilayer.²⁷

Similarly for the intracellular system, two C_{60} molecules were located at the intracellular side, near the pore entrance, and the other two C_{60} s were distributed near the NBDs (Fig. 5C and D). Fig. 6B shows a snapshot where we can see four C_{60} molecules bound to the surface of the P-gp during the 50 ns MD run. The nanoparticles are surrounded by seven carboxyl groups of hydrophobic residues (Val165, Val168, Pro402, Leu516, Pro517, Leu682, and Leu884) in P-gp. For the C_{60}^c locating itself near the NBD1, it exhibits a significant increase in mobility. It is evident from the Fig. 5C that C_{60}^c passes from the NBD2 to the cavity mouth of the P-gp during the first 2 ns of simulation. After that, the residue Val165 at the bottom of the cavity forms a nonleaky hydrophobic occlusion (Fig. 6B), and as a consequence forbids the penetration of C_{60}^c into the cavity of the protein.

As for the interior system, it considers C_{60} molecules distributed in the membrane interior, where two C_{60} s were located at opposite directions of the P-gp portals (Fig. 5E and F). During 50 ns of such a simulation, the C_{60} molecules bind closely to the membrane interior except for occasional movement around the portals of P-gp (e.g., at 6.6 ns, 9.2 ns, 11.7 ns, 18.2 ns), revealing no propensity of fullerenes to enter the protein portals.

To further elucidate the sensitivity of C_{60} transport to P-gp, two additional 20 ns MD simulations (systems (d) and (e)) on

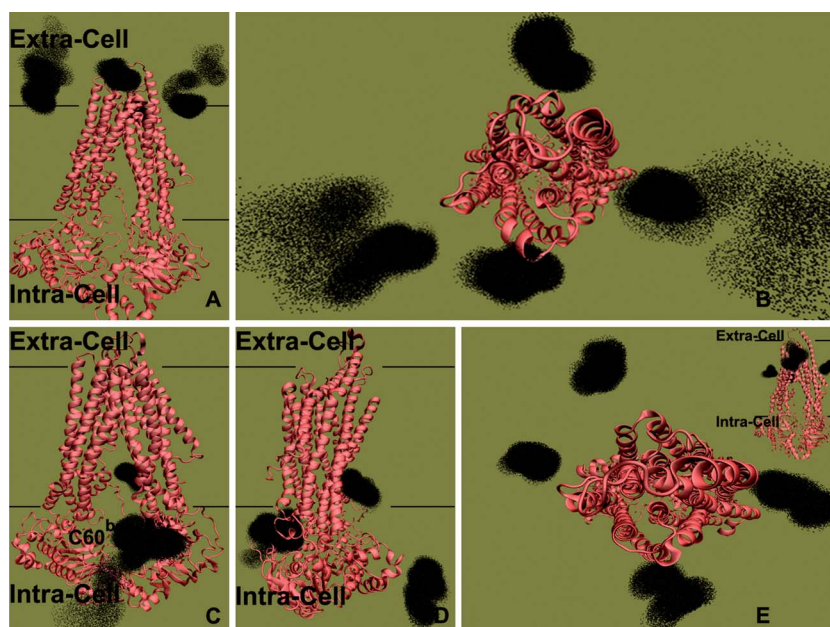


Fig. 5 C_{60} distribution surrounding P-gp. The dots represent the position of C_{60} along the MD trajectory sampled every 0.1 ns. (A) Side view with a highlight of aggregation of C_{60} to the extracellular part of P-gp. (B) Top view of (A). (C) Side view with a highlight of C_{60} distribution to the intracellular part of P-gp. (D) Top view of (C). (E) shows top view of P-gp with C_{60} distributing in the membrane interior. (F) Side view of (E). For clarity, the membrane lipids and the water molecules are not shown and only the protein is displayed.

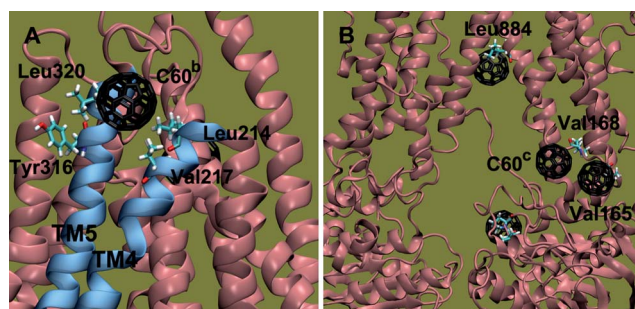


Fig. 6 P-gp with C_{60} placed in the extracellular (A) and intracellular (B) membranes. The protein and the C_{60} are drawn in pink and black, and residues are colored on the backbone (white for hydrogen, red for oxygen, blue for nitrogen and cyan for carbon). Membranes are left out for clarity.

Val165Ala, Pro402Ala, Arg680Ala mutants and on Asp167Ala, Val168Ala, Gly169Ala, Arg680Ala, Lys681Ala, Leu682Ala, Ser683Ala mutants are performed, respectively. Comparing Val165Ala, Pro402Ala, Arg680Ala with the wild type P-gp, the C_{60} migrate laterally toward membrane protein with distance of 3.5 Å, showing their propensity to migrate through the gate formed by loops 2–3 and 6–7 to the central cavity and towards their putative binding site (Fig. 7A). However, partial closing of the gate occurred with the movement of C_{60} (Fig. 7C), causing this nanoparticle to pause out of the cavity for the rest of the simulation time (~6 ns). While for the mutations to Ala in system (e), these mutations act as “glue” to adhere the C_{60} to loop 6–7 (Fig. 7B and D), leading to the inability of this nanoparticle to enter the P-gp cavity. In summary, the two MD simulations of C_{60} show the incapability to plug the entrance of P-gp.

3. Discussion

Biological defense systems against internal and external toxins are very old and efficient. As essential parts of an innate defense system, multidrug transporters, especially P-gp, are preserved throughout all living systems, from bacteria to human, and provide general protection against hydrophobic xenobiotics. Our work has addressed the potential P-gp defense against the typical nanoparticle C_{60} using a combined experimental and MD study. Although previous studies have shown that transferrin-conjugated nanoparticles and surfactant–polymer nanoparticles are capable of conquering drug resistance,^{38,39} the typical,

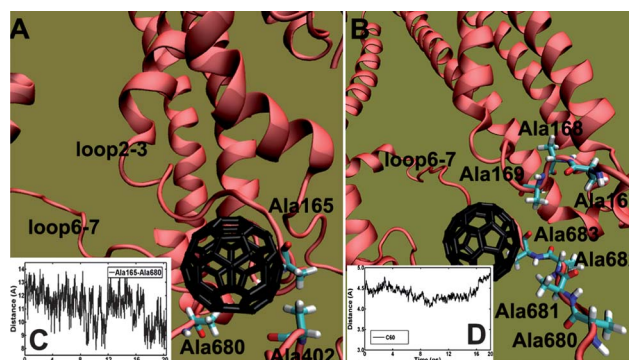


Fig. 7 Mutations to Ala in P-gp. (A) shows the failed migration of C_{60} through the gate formed by loops 2–3 and 6–7. (B) shows the adherence of C_{60} to the loop 6–7. (C) shows time evolution of the center-of-mass distance between Ala 165 and Ala 680 during the 20 ns MD simulation. (D) shows time evolution of the center-of-mass distance of C_{60} from the starting structure during the 20 ns MD simulation.

non-surface-modified and multifunctional nanoparticles were still not investigated.

In the investigation of whether C_{60} was a potential substrate for P-gp, we traced the fluorescent signs (AMF- C_{60}) to represent the ongoing transport process of C_{60} in the K562 cell model. Before this assay, we performed a control experiment to identify that the fluorescein (5-AMF) was unable to be recognized and energy-dependently removed by P-gp. In addition, we find that the relationship between fluorescence intensity (G_{mean}) and fluorescein concentration (C_{60}) is similar to that described previously, showing that the accumulation level of gold nanoparticles in drug-sensitive cells HepG2 and MDR cells HepG2-R increased in proportion to the nanoparticle dose from 3.75 to 15 μM .⁴⁰ This suggests the linear drug accumulation of K562R and K562S cells for C_{60} at relatively low concentrations. Indeed, the cellular accumulation is a result of a combined activity and equilibrium of uptake and efflux of small molecules. A previous study has shown that the cellular uptake of nanoparticles was mediated through energy-dependent endocytosis,¹⁹ which implies that the C_{60} uptake amount does not correlate with the P-gp expression level in the cells. It is thus clear that the nanoparticles can be effluxed from the two types of cells equally, and the degree of intracellular accumulation of C_{60} does not depend on the level of P-gp expression. These results provide reliable information for the application of nanoparticles for current cancer treatment, drug design, and drug development strategies,⁴¹ and also raise a question of why the nanoparticles have the capacity to conquer MDR.

It is well known that biological molecules can selectively cooperate with each other based on the complementarity between non-polar hydrophobic groups and polar interactions. Since nanoparticles have very unusual spatial structures and surface polarity properties, they should also cooperate with other molecules in a very unusual manner. For example, the face-centered-cubic C_{60} without polar groups is capable of specific interactions with antibodies.⁴² Previous studies have stated that the most important factors of nanoparticle-based interactions include van der Waals forces, hydrophobicity, π -interactions, and high spherical or cylindrical symmetry of nanoparticles, and more importantly, enthalpy driven effects of these factors for nanoparticles with other organic molecules were much larger than standard molecular systems.⁴³ Given this, one can therefore speculate that nanoparticles, especially C_{60} , might form hybrid bimolecular complexes with P-gp with relatively high binding affinities, and thus could not be pumped by the protein as normal substrates.

To further determine whether the C_{60} molecules possess P-gp inhibitor activity, we investigated the effect of blank nanoparticles on the accumulation of Rho 123. Because of the water insolubility of fullerenes, we used five doses (0, 10, 20, 30, 40 $\mu\text{g mL}^{-1}$) in this study. Previous studies have shown that 300 $\mu\text{g mL}^{-1}$ of surfactant-polymer nanoparticles enables the inhibition of P-gp-mediated drug efflux, leading to the enhanced cellular accumulation of Rho 123.³⁷ Contrary to this finding, no enhancement in cellular accumulation was observed in this work, even at the highest concentration of C_{60} .

In recent decades, P-gp inhibitors as suitable tools to reverse modulate or reverse MDR in cancer patients have been studied extensively.⁴⁴ They are found to block P-gp activity by

competition for drug-binding sites (competitive inhibitors) or by blocking the ATP hydrolysis process (noncompetitive inhibitors). In fact, the presence of multiple drug binding sites of P-gp has been proposed, and also, the H-site (binds Hoechst 33342) and the R-site (binds Rho 123) within P-gp have been described.⁴⁵ As our previous data has shown, C_{60} cannot inhibit the transport of Rho 123 efficiently and we can speculate that C_{60} could not bind to the same site as the fluorescent agent, *i.e.*, the R site, and thus, could not compete as a substrate with the agent for transport by P-gp. On the other hand, it is also probable that C_{60} does not have the capability to induce a conformational change in P-gp and prevent ATP hydrolysis and transport of Rho 123 out of the cell. However, the exact mechanism of why the nanoparticles do not inhibit P-gp activity *in vitro* has not been established in this report.

Molecular dynamics (MD), as one of the most powerful computational tools in simulations of biophysical systems,^{46–48} is able to provide links between structure and dynamics by enabling the exploration of the conformational energy landscape accessible to protein molecules. In this work, the simulation results show multiple C_{60} binding sites in the vicinity or interior of a model membrane which do not overlap with the putative sites (Ser222, Ile306, Leu339, Gly872, Ile868, Thr945, Val982) of P-gp identified in previous study.⁴⁹ It is well known that binding of a substrate or inhibitor to the high-affinity binding site results in ATP hydrolysis, causing a conformational change that shifts the substrate to a lower-affinity binding site and then releases it into the extracellular space. Thus, one can speculate that if the modulators did not occupy the binding sites of P-gp, they could not be transported by this protein. The results of the MD simulations are indeed in agreement with our previous experiments; C_{60} is not susceptible to P-gp mediated efflux transport, and cannot exert an inhibitory effect on P-gp-mediated efflux. Meanwhile, our result is also consistent with the observation of Tarek's group, which determined that C_{60} molecules initially located near the extracellular mouth of the bacterial KcsA channel reveal no propensity to anchor to or block the selectivity filter that delimites K^+ channels and allows these channels to discriminate K^+ from other cations.³⁰ The MD information clearly provides an insight into the possible mechanisms governing the recognition of C_{60} by P-gp and a molecular view on the capability of C_{60} to overcome resistance.

The above discussion suggests a relationship between the representative nanoparticle C_{60} and P-gp based on a combined experimental and theoretical study. From an evolutionary viewpoint, MDR-ABC transporters have evolved from early bacterial transporters dedicated to specific solute transport, initially using the energy derived from a preexisting electrochemical gradient.⁵⁰ Under survival pressures, they develop and deploy protecting countermeasures against xenobiotics, which requires an efficient and adaptable mechanism of action. Indeed, a whole-genome analysis has suggested that the ABC transporters evolved with higher than expected rates of duplication,⁵¹ indicating that these transporters are particularly adaptable evolutionary modules. Despite the high-altitude adaptation of these transporters, the initiation event for the recognition of xenobiotics should be the long-term exposure of cell tissue to these compounds that induces a continuing response of some cells in the tissue.⁵² Exogenous nanoparticles, although some of

them, including C₆₀, have existed on earth for a considerable time and even occur naturally, can only be released by combustion processes such as forest fires. Therefore, these nanoparticles have fewer effects on the fluctuation of environment due to their rare emergence. This finally gives rise to the complexity of functional adaptation of the ABC transporter P-gp and its failure of activation of stress responsiveness during evolution, *i.e.*, C₆₀ cannot be recognized by P-gp.

5. Conclusions

We presented *in vitro* cell assays in combination with theoretical methods to measure the recognition and transport of nanoparticles by P-gp. We demonstrated that the representative nanoparticle C₆₀ could not be efficiently effluxed by the P-gp protein, and in turn was not capable of inhibiting the P-gp-mediated efflux of the model substrate Rho-123 across the cellular membrane. Homology modeling and MD simulations for C₆₀ molecules distributing in the extracellular, intracellular and interior of the bilayer were further carried out to complement the experimental findings. It is noted that until recently the information about the recognition between the simple, non-modified and multifunctional nanoparticles and P-gp has not been available. The information in this work is thus clearly essential for the development of advanced drug delivery systems, involving enhancing the therapeutic efficacy of antitumor drugs, and controlling the release of anti-cancer drugs to achieve pharmacologically effective concentrations in the cells.

Acknowledgements

The research is supported by high-performance computing platform of Northwest A & F University, the Fund of Northwest A & F University and is financially supported by the National Natural Science Foundation of China (Grant No. 31170796).

References

- 1 S. Geffeny, E. D. Brodie, P. C. Ruben and E. D. Brodie, Mechanisms of adaptation in a predator-prey arms race: TTX-resistant sodium channels, *Science*, 2002, **297**(5585), 1336–1339.
- 2 R. W. Johnstone, A. A. Ruefli and M. J. Smyth, Multiple physiological functions for multidrug transporter P-glycoprotein?, *Trends Biochem. Sci.*, 2000, **25**(1), 1–6.
- 3 A. T. Fojo, K. Ueda, D. J. Slamon, D. G. Poplack, M. M. Gottesman and I. Pastan, Expression of a multidrug-resistance gene in human tumors and tissues, *Proc. Natl. Acad. Sci. U. S. A.*, 1987, **84**, 265–269.
- 4 K. Ueda, C. Cardarelli, M. M. Gottesman and I. Pastan, Expression of a full-length cDNA for the human “MDR1” gene confers resistance to colchicine, doxorubicin, and vinblastine, *Proc. Natl. Acad. Sci. U. S. A.*, 1987, **84**, 3004–3008.
- 5 P. Gros, Y. B. Ben Neriah, J. M. Croop and D. E. Housman, Isolation and expression of a complementary DNA that confers multidrug resistance, *Nature*, 1986, **323**, 728–731.
- 6 J. H. Gerlach, J. A. Endicott, P. F. Juranka, G. Henderson, F. Sarangi, K. L. DeucAars and V. Ling, Homology between P-glycoprotein and a bacterial haemolysin transport protein suggests a model for multidrug resistance, *Nature*, 1986, **324**, 485–489.
- 7 X. Xu, J. Fu, H. Wang, B. Zhang, X. Wang and Yh. Wang, Influence of P-glycoprotein on embryotoxicity of the antifouling 4 biocides to sea urchin (*Strongylocentrotus intermedius*), *Ecotoxicology*, 2011, **20**(2), 419–428.
- 8 K. Terasaka, J. J. Blakeslee, B. Titapiwatanakun, W. A. Peer, A. Bandyopadhyay, S. N. Makam, O. R. Lee, E. L. Richards, A. S. Murphy, F. Sato and K. Yazaki, PGP4, an ATP binding

- cassette P-glycoprotein, catalyzes auxin transport in *Arabidopsis thaliana* roots, *Plant Cell*, 2005, **17**, 2922–2939.
- 9 Y. H. Wang, Y. Li, S. L. Yang and L. Yang, Classification of substrates and inhibitors of P-glycoprotein using unsupervised machine learning approach, *J. Chem. Inf. Model.*, 2005, **45**(3), 750–757.
- 10 J. K. Vasir and V. Labhasetwar, Targeted drug delivery in cancer therapy, *Technology in Cancer Research and Treatment*, 2005, **4**, 363–374.
- 11 J. S. Ross, D. P. Schenkein, R. Pietrusko, M. Rolfe, G. P. Linette, J. Stec, N. E. Stagliano, Ginsburg, W. F. Symmans, L. Pusztai and G. N. Hortobagyi, Targeted therapies for cancer 2004, *Am. J. Clin. Pathol.*, 2004, **122**, 598–609.
- 12 T. Xia, N. Li and A. E. Nel, Potential health impact of nanoparticles, *Annu. Rev. Public Health*, 2009, **30**, 137–150.
- 13 H. J. Johnston, G. R. Hutchison, F. M. Christensen, K. Aschberger and V. Stone, The biological mechanisms and physicochemical characteristics responsible for driving fullerene toxicity, *Toxicol. Sci.*, 2010, **114**(2), 162–182.
- 14 G. K. Bonn, R. Bakry, R. M. Vallant, M. Najam-ul-Haq, M. Rainer, Z. Szabo and C. W. Huck, Medicinal applications of fullerenes, *International Journal of Nanomedicine*, 2007, **2**(4), 639–649.
- 15 L. E. Murr, E. V. Esquivel, J. J. Bang, G. de la Rosa and J. L. Gardea-Torresdey, Chemistry and nanoparticle compositions of a 10,000 year-old ice core melt water, *Water Res.*, 2004, **38**, 4282–4296.
- 16 F. E. Koehn and G. T. Carter, The evolving role of natural products in drug discovery, *Nat. Rev. Drug Discovery*, 2005, **4**, 206–220.
- 17 R. B. Li, R'A Wu, L. Zhao, M. H. Wu, L. Yang and H. F. Zou, P-Glycoprotein antibody functionalized carbon nanotube overcomes the multidrug resistance of human Leukemia cells, *ACS Nano*, 2010, **4**(3), 1399–1408.
- 18 M. J. Later, E. M. Amphlett, D. M. Andrews, G. Bravi, G. Burton, A. G. Cheasty, J. A. Corfield, M. R. Ellis, R. H. Fenwick, S. Fernandes, R. Guidetti, D. Haigh, C. D. Hartley, P. D. Howes, D. L. Jackson, R. L. Jarvest, V. L. Lovegrove, K. J. Medhurst, N. R. Parry, H. Price, P. Shah, O. M. Singh, R. Stocker, P. Thommes, C. Wilkinson and A. Wonacott, Optimization of novel acyl pyrrolidine inhibitors of hepatitis C virus RNA-dependent RNA polymerase leading to a development candidate, *J. Med. Chem.*, 2007, **50**, 897–900.
- 19 T. Schwede, J. Kopp, N. Guex and M. C. Peitsch, SWISS-MODEL: An automated protein homology-modeling server, *Nucleic Acids Res.*, 2003, **31**, 3381–3385.
- 20 R. W. Hoofst, G. Vriend, C. Sander and E. E. Abola, Errors in protein structures, *Nature*, 1996, **381**, 272–272.
- 21 H. Heller, M. Schaefer and K. Schulten, Molecular dynamics simulation of a bilayer of 200 lipids in the gel and in the liquid crystal-phases, *J. Phys. Chem.*, 1993, **97**, 8343–8360.
- 22 L. Islas and F. Sigworth, Electrostatics and the gating pore of shaker potassium channels, *J. Gen. Physiol.*, 2001, **117**, 69–89.
- 23 S. G. Aller, J. Yu, A. Ward, Y. Weng, S. Chittaboina, R. Zhuo, P. M. Harrell, Y. T. Trinh, I. L. Urbatsch and G. Chang, Structure of P-Glycoprotein reveals a molecular basis for poly-specific drug binding, *Science*, 2009, **323**(5922), 1718–1722.
- 24 A. D. MacKerell Jr, D. Bashford, M. Bellott, R. L. Dunbrack Jr, J. D. Evanseck, M. J. Field, S. Fischer, J. Gao, H. Guo, S. Ha, D. Joseph-McCarthy, L. Kuchnir, K. Kuczera, F. T. K. Lau, C. Mattos, S. Michnick, T. Ngo, D. T. Nguyen, B. Prodhom, W. E. Reiher III, B. Roux, M. Schlenker, J. C. Smith, R. Stote, J. Straub, M. Watanabe, J. Wiorkiewicz-Kuczera, D. Yin and M. Karplus, All-atom empirical potential for molecular modeling and dynamics studies of proteins, *J. Phys. Chem. B*, 1998, **102**(18), 3586–3616.
- 25 L. A. Girifalco, Molecular properties of C₆₀ in the gas and solid phases, *J. Phys. Chem.*, 1992, **96**, 858–861.
- 26 J. C. Phillips, R. Braun, W. Wang, J. Gumbart, E. Tajkhorshid, E. Villa, C. Chipot, R. D. Skeel, L. Kale and K. J. Schulten, Scalable molecular dynamics with NAMM, *J. Comput. Chem.*, 2005, **26**, 1781–1802.
- 27 A. D. MacKerell, N. Banavali and N. Foloppe, Development and current status of the CHARMM force field for nucleic acids, *Biopolymers*, 2000, **56**, 257–265.
- 28 A. D. MacKerell Jr., M. Feig and C. L. Brooks III, Extending the treatment of backbone energetics in protein force fields: Limitations of gas-phase quantum mechanics in reproducing protein

- conformational distributions in molecular dynamics simulations, *J. Comput. Chem.*, 2004, **25**, 1400–1415.
- 29 U. Essmann, L. Perera, M. L. Berkowitz, T. Darden, H. Lee and L. G. Pedersen, A smooth particle mesh Ewald method, *J. Comput. Phys.*, 1995, **103**, 8577–8593.
- 30 J. P. Ryckaert, G. Ciccotti and H. J. C. Berendsen, Numerical integration of the cartesian equations of motion of a system with constraints: molecular dynamics of *n*-alkanes, *J. Comput. Phys.*, 1977, **23**, 327–341.
- 31 H. C. Andersen, Rattle: a “velocity” version of the shake algorithm for molecular dynamics calculations, *J. Comput. Phys.*, 1983, **52**, 24–34.
- 32 C. W. Isaacson, C. Y. Usenko, R. L. Tanguay and J. A. Field, Quantification of fullerenes by LC/ESI-MS and its application to in vivo toxicity assays, *Anal. Chem.*, 2007, **79**, 9091–9097.
- 33 D. L. Cox and J. D. Radolf, Insertion of fluorescent fatty acid probes into the outer membranes of the pathogenic spirochaetes *Treponema pallidum* and *Borrelia burgdorferi*, *Microbiology*, 2001, **147**, 1161–1169.
- 34 I. C. van der Sandt, M. C. Blom-Roosemalen, A. G. de Boer and D. D. Breimer, Specificity of doxorubicin versus rhodamine-123 in assessing P-glycoprotein functionality in the LLC-PK1, LLC-PK1:MDR1 and Caco-2 cell lines, *Eur. J. Pharm. Sci.*, 2000, **11**, 207–214.
- 35 P. P. Annaert and K. L. R. Brouwer, Assessment of drug interactions in hepatobiliary transport using Rhodamine-123 in sandwich-cultured rat hepatocytes, *Drug Metab. Dispos.*, 2004, **33**(3), 388–394.
- 36 P. Pavek, F. Staud, Z. Fendrich, H. Sklenarova, A. Libra, M. Novotna, M. Kopecky, M. Nobilis and V. Semecky, Examination of the functional activity of P-glycoprotein in the rat placental barrier using Rhodamine 123, *J. Pharmacol. Exp. Ther.*, 2003, **305**(3), 1239–1250.
- 37 H. A. Namanja, D. Emmert, M. M. Pires, C. A. Hrycyna and J. Chmielewski, Inhibition of human P-glycoprotein transport and substrate binding using a galantamine dimer, *Biochem. Biophys. Res. Commun.*, 2009, **388**(4), 672–676.
- 38 S. K. Sahoo and V. Labhasetwar, Enhanced antiproliferative activity of transferrin-conjugated paclitaxel-loaded nanoparticles is mediated via sustained intracellular drug retention, *Mol. Pharmaceutics*, 2005, **2**, 373–383.
- 39 M. D. Chavanpatil, A. Khair, B. Gerard, C. Bachmeier, D. W. Miller, M. P. V. Shekhar and J. Panyam, Surfactant-polymer nanoparticles overcome P-glycoprotein-mediated drug efflux, *Mol. Pharmaceutics*, 2007, **4**(5), 730–738.
- 40 Y. J. Gu, J. Cheng, C. W. Y. Man, W. T. Wong and S. H. Cheng, Gold-doxorubicin nanoconjugates for overcoming multidrug resistance, *Nanomedicine: Nanotechnology, Biology, and Medicine*, 2011 in Press.
- 41 M. M. Gottesman, T. Fojo and S. E. Bates, Multidrug resistance in cancer: role of ATP-dependent transporters, *Nat. Rev. Cancer*, 2002, **2**, 48–58.
- 42 B.-X. Chen, S. R. Wilson, M. Das, D. J. Couglin and B. F. Erlanger, Antigenicity of fullerenes: antibodies specific for fullerenes and their characteristics, *Proc. Natl. Acad. Sci. U. S. A.*, 1998, **95**, 10809–10813.
- 43 S. Kozyrev and P. Yakutseni, Nanocarbon technologies: prospects and risks, *NATO Sci. Peace Secur. Ser. B: Phys. Biophys.*, 2009, 9–18.
- 44 A. Aszalos, Drug–drug interactions affected by the transporter protein, P-glycoprotein (ABCB1, MDR1): II. Clinical aspects, *Drug Discovery Today*, 2007, **12**(19–20), 838–843.
- 45 A. B. Shapiro and V. Ling, Positively cooperative sites for drug transport by P-glycoprotein with distinct drug specificities, *Eur. J. Biochem.*, 1997, **250**, 130–137.
- 46 X. Xu, X. Wang, Z. Xiao, Y. Li and Y. Wang, Two TPX2-dependent switches control the activity of Aurora A, *Plos one*, 2011, **6**(2), 1–7.
- 47 X. Xu, W. Yang, X. Wang, Y. Li, Y. Wang and C. Ai, Dynamic communication between androgen and coactivator: mutually induced conformational perturbations in androgen receptor ligand-binding domain, *Proteins: Struct., Funct., Bioinf.*, 2011, **79**(4), 1154–1171.
- 48 A. L. Milac1, N. V. Buchete, T. A. Fritz1, G. Hummer and L. A. Tabak, Substrate-induced conformational changes and dynamics of UDP-N-Acetylgalactosamine: Polypeptide N-Acetylgalactosaminyltransferase-2, *J. Mol. Biol.*, 2007, **373**, 439–451.
- 49 T. W. Loo and D. M. Clarke, Determining the dimensions of the drug-binding domain of human P-glycoprotein using thiol cross-linkers as molecular rulers, *J. Biol. Chem.*, 2001, **276**, 36877–36880.
- 50 H. Venter, R. A. Shilling, S. Velamakanni, L. Balakrishnan and H. W. Van Veen, An ABC transporter with a secondary-active multidrug translocator domain, *Nature*, 2003, **426**, 866–870.
- 51 J. A. Sheps, S. Ralph, Z. Zhao, D. L. Baillie and V. Ling, The ABC transporter gene family of *Caenorhabditis elegans* has implications for the evolutionary dynamics of multidrug resistance in eukaryotes, *Genome Biology*, 2004, **5**(3), R15.
- 52 T. V. Karpinets and B. D. Foy, Tumorigenesis: the adaptation of mammalian cells to sustained stress environment by epigenetic alterations and succeeding matched mutations, *Carcinogenesis*, 2005, **26**(8), 1323–1334.